Analysis of rainfall-induced slope instability using a field of local factor of safety

Ning Lu,[1] Başak Şener-Kaya,[1] Alexandra Wayllace,[1] and Jonathan W. Godt[2]

Received 4 January 2012; revised 24 July 2012; accepted 25 July 2012; published 18 September 2012.

[1] Slope-stability analyses are mostly conducted by identifying or assuming a potential failure surface and assessing the factor of safety (FS) of that surface. This approach of assigning a single FS to a potentially unstable slope provides little insight on where the failure initiates or the ultimate geometry and location of a landslide rupture surface. We describe a method to quantify a scalar field of FS based on the concept of the Coulomb stress and the shift in the state of stress toward failure that results from rainfall infiltration. The FS at each point within a hillslope is called the local factor of safety (LFS) and is defined as the ratio of the Coulomb stress at the current state of stress to the Coulomb stress of the potential failure state under the Mohr-Coulomb criterion. Comparative assessment with limit-equilibrium and hybrid finite element limit-equilibrium methods show that the proposed LFS is consistent with these approaches and yields additional insight into the geometry and location of the potential failure surface and how instability may initiate and evolve with changes in pore water conditions. Quantitative assessments applying the new LFS field method to slopes under infiltration conditions demonstrate that the LFS has the potential to overcome several major limitations in the classical FS methodologies such as the shape of the failure surface and the inherent underestimation of slope instability. Comparison with infinite-slope methods, including a recent extension to variably saturated conditions, shows further enhancement in assessing shallow landslide occurrence using the LFS methodology. Although we use only a linear elastic solution for the state of stress with no post-failure analysis that require more sophisticated elastoplastic or other theories, the LFS provides a new means to quantify the potential instability zones in hillslopes under variably saturated conditions using stress-field based methods.

Citation: Lu, N., B. Şener-Kaya, A. Wayllace, and J. W. Godt (2012), Analysis of rainfall-induced slope instability using a field of local factor of safety, *Water Resour. Res.*, *48*, W09524, doi:10.1029/2012WR011830.

1. Introduction

[2] Slope-stability analyses are commonly performed using limit-equilibrium methods because of their proven effectiveness and reliability [e.g., *Fellenius*, 1936; *Bishop*, 1955; *Morgenstern and Price*, 1965; *Janbu*, 1973; *Lade*, 1992; *Michalowski*, 2002; *Duncan and Wright*, 2005]. For such methods, the geometry and sometimes the location of the potential failure surface are approximated or predetermined. All two-dimensional limit-equilibrium methods consist of discretizing the mass of a potential failure slope into smaller vertical slices. All limit-equilibrium methods assume that each individual slice is treated as a unique sliding block (as shown in Figure 1a) and shear strength is mobilized with the same ratio of shear stress to shear strength for all slices.

[3] By applying the principles of force and/or moment equilibrium, all limit-equilibrium methods seek an indicator of slope stability called the "factor of safety" or FS, which is typically defined as the ratio of the available shear strength to the shear stress required for equilibrium along the prescribed failure surface. Depending on how interslice forces are handled and the equilibrium principles that are involved, many variations of limit-equilibrium methods have been developed. For later comparison with the new method proposed in this work, the commonalities and differences among these classical methods are illustrated in Figure 1 and summarized below.

[4] The Ordinary Method (Figure 1b) [*Fellenius*, 1936] is the simplest and the oldest method of slices. It ignores all the inter-slice forces because of the assumption that the forces are parallel to the base of each slice. The method satisfies only moment equilibrium and assumes a circular slip surface. Due to its simplicity, it is possible to compute the factor of safety by hand calculations. The ordinary method is generally less accurate compared to the other methods of slices. In some studies [e.g., *Duncan and Wright*, 2005; *Fredlund and Krahn*, 1977; *Abramson et al.*, 1996], it has been shown that the

[1]Department of Civil and Environmental Engineering, Colorado School of Mines, Golden, Colorado, USA.
[2]Geologic Hazards Science Center, U.S. Geological Survey, Denver, Colorado, USA.

Corresponding author: N. Lu, Department of Civil and Environmental Engineering, Colorado School of Mines, Golden, CO 80401, USA. (ninglu@mines.edu)

0043-1397/12/2012WR011830

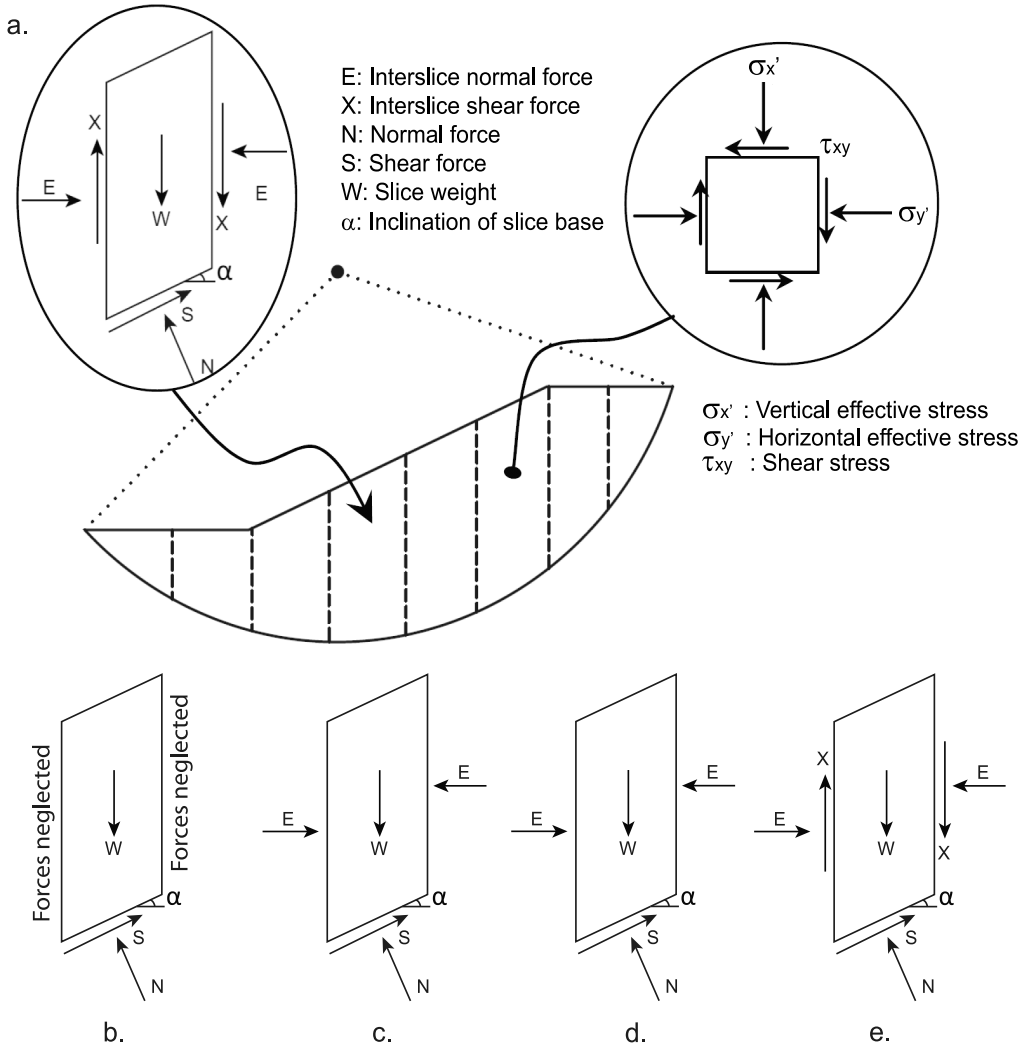

Figure 1. (a) Slice discretization of a potential sliding mass and forces acting on a typical slice used in limit-equilibrium methods. Illustration of the commonalities and differences among the classical methods of slices for (b) Ordinary (Fellenius) Method, (c) Bishop's Simplified Method (vertical force equilibrium), (d) Janbu's Simplified Method (horizontal force equilibrium), and (e) Morgenstern-Price Method.

accuracy is decreased for effective stress analyses and under high pore water pressure conditions.

[5] Bishops's simplified method (Figure 1c) [*Bishop*, 1955] satisfies vertical force equilibrium for each slice and overall moment equilibrium at the center of the circular trial surface (Figure 1a). The method also ignores inter-slice shear forces (X). Bishop's simplified method is considered to be more accurate than the Ordinary method, especially for effective stress analyses with high pore water pressures [e.g., *Duncan and Wright*, 2005; *Abramson et al.*, 1996].

[6] The Janbu Simplified Method (Figure 1d) satisfies only overall horizontal force equilibrium and also assumes that there are no interslice shear forces (X). The assumption that all the interslice forces are horizontal often leads to smaller factor of safety when compared to more rigorous methods that satisfy complete force and moment equilibrium. To account for the effect of the shear forces, a correction factor related to cohesion, angle of friction and the shape of the failure surface were presented by Janbu [e.g., *Duncan and Wright*, 2005; *Abramson et al.*, 1996].

[7] The Morgenstern and Price Method (Figure 1e, 1965) considers both shear (X) and normal (E) interslice forces and satisfies both moment and force equilibrium. The method assumes an arbitrary mathematical function to describe the direction of the interslice forces [e.g., *Fredlund and Krahn*, 1977].

[8] Some recent developments of methods to calculate the factor of safety include more accurate computation of the interslice stress distributions [*e.g.*, *Duncan*, 1996; *Yu et al.*, 1998; *Swan and Seo*, 1999] and numerical algorithms for shear strength reduction analysis from finite element methods for multidimensional analysis under a continuum mechanics framework [e.g., *Matsui and San*, 1992; *Smith and Griffiths*, 2004; *Krahn*, 2003]. The classical limit-equilibrium methods described above and a hybrid FEM-limit equilibrium method [*Krahn*, 2003; *GEO-SLOPE International*, 2007] represent

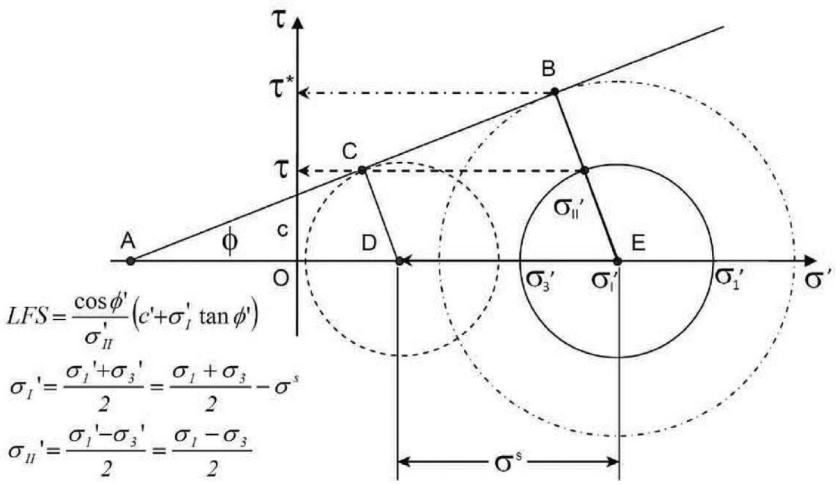

Figure 2. Illustration of the concept of a scalar field of local factor of safety. The current state of stress at any point in hillslope (shown as the solid-line circle) has a shear stress τ and shear strength τ*. The quantity τ^*/τ can be used as an indicator of how far the current state of stress is from failure and is defined as the local factor of safety (LFS). If suction stress σ^s is reduced at this point, the circle shifts leftward and the LFS is reduced, indicating that the state of stress is closer to the failure condition or LFS = 1.0.

the state-of-the-art in slope stability analysis and will be used in what follows for comparison with the new LFS method.

[9] Because limit-equilibrium and stress-field based methods typically seek a single stability indicator for the entire slope, they provide little insight into the location of initial failure and how the region of potential instability evolves with changes in pore water conditions that accompany rainfall infiltration. We describe a method to calculate a scalar field of factor of safety to overcome some of these limitations and take full advantage of modern numerical solutions for variably saturated flow and the state of stress in hillslopes.

2. Definition of the Scalar Field (or Local) of Factor of Safety

[10] The basic idea is to seek a scalar quantity at each point in a hillslope that is indicative of stability at that point. Our method extends the approach described by *Iverson and Reid* [1992] to cohesive, variably saturated porous material and uniquely provides a physically meaningful quantity to assess the stability of partially saturated hillslopes. As illustrated in two-dimensional stress space in Figure 2, if the current state of stress at a point of interest is the solid circle, the stress quantity τ indicates of the state of failure. This stress τ can be uniquely defined by shifting the Mohr circle leftward until it touches the Mohr-Coulomb (M-C) failure envelope. *King et al.* [1994] called the shear stress on the Mohr circle along the direction perpendicular to the M-C failure criterion "Coulomb stress." Scalar fields of Coulomb stress calculated in this manner near faults have been used to understand the state of stress in the Earth's crust and the occurrence of earthquake aftershocks [e.g., *Toda et al.*, 1998]. The paths of changes in effective stress in slopes that result from changes in pore water conditions follow a similar leftward shift. The size of the Mohr circle remains nearly constant under changing pore water conditions because the size of the Mohr circle is determined by the difference in principal total stresses. The principal total stresses are mainly affected by the geometry of the slope and self-weight of slope materials. The former does not change for a given slope over timescales relevant to rainfall infiltration and changes in the latter are relatively small compared with changes in pore water pressure and effective stress during rainfall infiltration and seepage that lead to a leftward shift of the Mohr circle.

[11] The pattern of the shift in the stress path implies that the direction of failure under variably saturated soil conditions would be similar to the direction of Coulomb stress. If the reference point for soil strength at the current state of stress (the solid Mohr circle) can be estimated by the intercept of the extension of the Coulomb stress with the M-C envelope, shown as point *B* in Figure 2, a local factor of safety (LFS) at each point within the entire slope can be defined as

$$LFS = \frac{\tau^*}{\tau} \tag{1}$$

where τ* is the potential Coulomb stress and τ is the current state of Coulomb stress. By the similarity of triangles *ACD* and *ABE*, the LFS can be expressed conveniently in terms of the ratio of the adjusted mean stress of the current state of stress to the adjusted mean stress of the potential failure state under the Mohr-Coulomb criterion. The adjustment here comes from the fact that hillslope materials are typically cohesive and tensile stresses could occur in the area near the slope crest. To include such a situation, a stress value of *AD*, in lieu of the stress invariant *OD* (Figure 2) is used. Similarly, a stress value of *AE* in lieu of the stress invariant *OE* is used. Graphically, the LFS defined by equation (1) is equal to

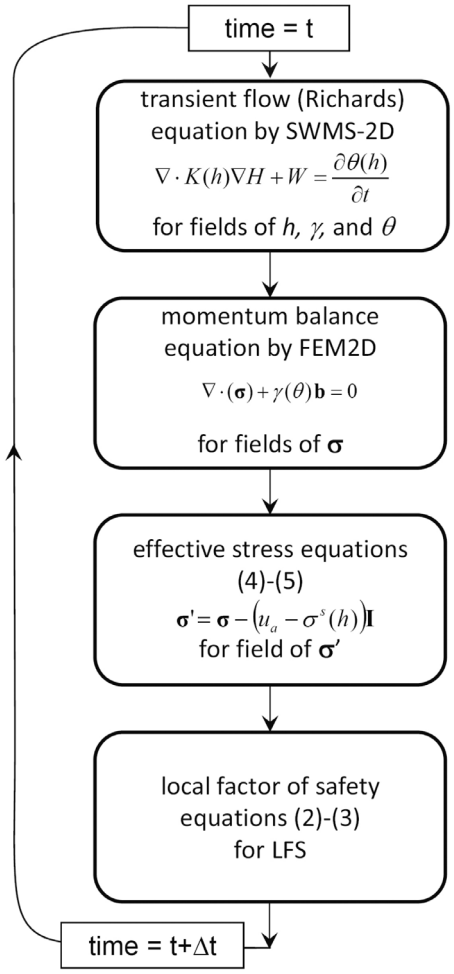

Figure 3. Illustration of the time-matching scheme in the one-way coupled hydro-mechanical framework in HILLSLOPE $(FS)^2$.

AE over *AD*. If the Mohr-Coulomb failure criterion is used, it can be shown that

$$LFS = \frac{2\cos\phi'}{q'}(c' + p'\tan\phi') \tag{2}$$

where c' is the drained cohesion of the slope material, ϕ' is the drained friction angle of the slope material, p' and q' are the mean and deviator effective stresses in two-dimensional space, respectively, and are defined by

$$p' = \frac{\sigma_1' + \sigma_3'}{2} = \frac{\sigma_1 + \sigma_3}{2} - \sigma^s \tag{3a}$$

$$q' = \sigma_1' - \sigma_3' = \sigma_1 - \sigma_3 \tag{3b}$$

with the generalized effective stresses for variably saturated porous media defined by suction stress σ^s [*Lu and Likos*, 2004, 2006] as

$$\sigma_1' = \sigma_1 - u_a - \sigma^s \tag{4a}$$

$$\sigma_3' = \sigma_3 - u_a - \sigma^s \tag{4b}$$

where u_a is the prevailing air pressure. Suction stress σ^s is a characteristic scalar function of a soil and varies with soil suction or saturation. It is equal to the pore water pressure when soil is fully saturated but generally smaller than the pore water pressure in partially saturated soil. Suction stress follows different patterns in clay, silt, and sand but can be unified in a single closed form for all soils [*Lu and Likos*, 2004, *Lu and Griffiths*, 2004, *Lu et al.*, 2010b] using the same set of parameters to describe soil-water characteristic curves in *van Genuchten*'s [1980] model, i.e.,

$$\sigma^s = -(u_a - u_w) \qquad u_a - u_w \le 0 \tag{5a}$$

$$\sigma^s = -\frac{(u_a - u_w)}{(1 + [\alpha(u_a - u_w)]^n)^{(n-1)/n}} \qquad u_a - u_w \ge 0 \tag{5b}$$

where α and n are unsaturated soil parameters identical to those in *van Genuchten*'s [1980] soil-water characteristic curve model that relates the equivalent moisture content θ_e (equals to the volumetric water content θ normalized by the residual water content θ_r) to soil suction $(u_a - u_w)$:

$$\theta_e = \frac{\theta - \theta_r}{1 - \theta_r} = \left\{\frac{1}{1 + [\alpha(u_a - u_w)]^n}\right\}^{1-1/n} \tag{6}$$

[12] Thus, in slopes the LFS so defined by equations (1)–(5) is a scalar quantity that varies in both space and time. As illustrated in Figure 2, if the state of stress in a slope represented by the Mohr circle is below the material's failure envelope, the LFS is greater than unity. Whereas for those zones in a slope with LFSs equal to unity, the states of stress have reached their limit states and local failure occurs. Therefore, LFS has the potential to delineate zones of stability or failure in slopes.

3. A Coupled Hydromechanical Framework

[13] To compute the fields of stresses, soil suction and saturation, and the LFS in a two-dimensional slope, a transient finite element framework was used. The code simulates one-way coupled variably saturated flow and stress problems using finite elements (FEM) for hillslope flow and stress and factor of safety (HILLSLOPE FS^2). The code was developed and validated by the authors [*Lu et al.*, 2010a] and was built from two previously uncoupled FEM codes (Figure 3). Both of the component codes were tested and validated by the original developers. The solution for transient unsaturated flow (Richards' equation) is based on the U.S. Department of Agriculture model SWMS_2D [*Simunek et al.*, 1994]. The Richards equation is [e.g., *Freeze and Cherry*, 1979; *Lu and Likos*, 2004]

$$\nabla \cdot K(h)\nabla H + W = \frac{\partial \theta(h)}{\partial t} \tag{7}$$

where *K(h)* is hydraulic conductivity function (HCF), *h* is pressure or suction head, *H* is total head ($H = h + z$), *W* is flux from a source or to a sink, and θ *(h)* is volumetric moisture content function commonly called the soil-water retention curve (SWRC). In general, *K(h)* and θ *(h)* are nonlinear functions of pressure head *h*. *Van Genuchten*'s

[1980] model shown in equation (6) is used for SWRC. *Mualem*'s [1976] is used for HCF.

$$k = k_s \frac{\left\{1 - (\alpha|h|)^{n-1}[1 + (\alpha|h|)^n]^{\frac{1}{n}-1}\right\}^2}{\{1 + [\alpha|h|]^n\}^{\frac{1}{2}-\frac{1}{2n}}} \quad (8)$$

where k_s is saturated hydraulic conductivity.

[14] Solutions of the transient fields of suction head h (or matric suction $(u_a - u_w)/\gamma$), moist unit weight γ, and moisture content θ are used as the coupling variables for the subsequent computation of the fields of total stress, suction stress, and LFS. The solutions for stress and displacement are based on FEM2D [*Reddy*, 1985] and use the field of moist unit weight as the gravity term. The total stresses in the slope are mainly affected by the geometry of the slope and the hillslope material's self-weight. The governing equations describing the total stresses in linear-elastic materials are from balance of linear momentum:

$$\nabla \cdot (\boldsymbol{\sigma}) + \gamma \mathbf{b} = 0 \quad (9)$$

where $\boldsymbol{\sigma}$ is a stress tensor with three independent stress variables in two-dimensional space, γ is the bulk unit weight of hillslope materials, and **b** is the unit vector of body forces with two components.

[15] The fields of total stress and suction head are then combined to compute a field of suction stress (Figure 3), and finally the total stress field and suction stress field are used to compute the field of LFS.

[16] Because plane-strain linear elasticity theory is implemented in FEM2D [*Reddy*, 1985], only two elastic properties, namely the elastic modulus E and Poisson's ratio v, are needed for solutions of both stress and displacement. Two unsaturated hydromechanical properties, namely α and n, are commonly defined in equations (5), (6), or (8). Additional modifications to the code include improved computational capacity and efficiency of the equation solver, addition of an automatic mesh generator, and graphical input and output.

[17] Comparisons of simulation results of suction head and stress fields with those obtained from a commercial slope-stability software package GeoStudio [*GEO-SLOPE International*, 2007] were made and close agreement between the two codes were obtained. For all the hybrid FEM-limit equilibrium analyses and the classical limit-equilibrium methods described in the following sections, SLOPE/W [*GEO-SLOPE International*, 2007] was also used.

[18] We point out that the hydromechanical framework based on linear elasticity solves statically admissible fields of stress and displacement without invoking failure or the redistribution of postfailure stress or displacement. A statically admissible stress distribution is defined only as one that satisfies the equilibrium differential equations, in the interior of the body, and the boundary conditions wherever any boundary tractions are prescribed [*Malvern*, 1969]. Thus LFS less than unity only provide an indication of hypothetical failure or the stress state in comparison with the hypothetical failure parameters, namely drained cohesion c' and angle of internal friction ϕ'. This simple computational strategy is used to illustrate the location of potential failure zones without involving more sophisticated statically indeterminate elastoplasticity theories. For this reason, in figures showing contours of the LFS, no distinction is made for computed LFS less than unity.

[19] In what follows, we first compare the LFS with several limit-equilibrium methods for stability analysis of slopes of various geometries under either dry or saturated and fully drained conditions. The potential applicability of the LFS to slope-stability analysis under variably saturated conditions is then explored for an example slope under transient rainfall conditions and followed with comparisons to some recent developments of infinite slope-stability theory under transient infiltration conditions.

4. Comparisons With the Classical Factor of Safety Methodologies

4.1. FS and LFS in Vertical Cuts

[20] We first compute the stress distribution in a vertical cut of either dry or saturated, but fully drained soil, under gravity for four different stability numbers m (0.05, 0.10, 0.15, and 0.20). The stability number is defined as $m = c'/\gamma H$ with γ being the unit weight of the slope material, and H the height of the slope. The internal friction angle ϕ' is assumed to be 30° in all cases here. A small m value indicates the slope is less stable compared to those with large m values. Based on the fields of stresses and strength parameters of the slope, the field of LSF is computed by equation (2) and plotted in Figure 4 (left). It can be seen that there are three weak or potentially unstable zones in a vertical cut slope from Figure 4a; near the vertical face, beneath the toe, and far field from the slope at the same elevation as the toe on horizontal ground. The low LFS zone behind the vertical face is characterized by the principal maximum stress in the vertical direction, whereas the low LFS zones beneath the toe and far field from the slope are characterized by the principal maximum stress in the horizontal direction. For all the m values examined here except for $m = 0.05$ (Figure 4a), the LFS in the far field area away from the slope is never below 1.0, whereas the LFS in the other two zones could be below 1.0 and the area expands as the m value decreases (Figure 4, left). The most pronounced weak zone is behind the vertical face with an up-leftward trend approximately 60° (or $\frac{\pi}{4} + \frac{\phi'}{2} = 60°$) from horizontal as the m value decreases (Figure 4a).

[21] To better illustrate this trend, contours of LFS equal to 1.0 are plotted in the right column in Figure 4 (thick solid lines) together with other potential failure surfaces identified by the four limit-equilibrium stability methods from the SLOPE/W software. To broaden the comparison and assessment, potential failure surfaces predicted by the Culmann method [*Culmann*, 1875; *Lohnes and Handy*, 1968] (analytical solution for finite slopes with a plane failure surface), and a global FS calculated using an FEM stress solution combined with a method of slices and iterative-search procedure to identify the least stable failure surface (Global method from SLOPE/W) are also plotted in Figure 4 (right).

[22] For a relatively strong vertical cut (m = 0.20 and shown in Figure 4d), all four limit-equilibrium methods (Ordinary, Bishop, Janbu, and Morgenstern-Price), as well as the Culmann and Global methods, predict that the vertical cut is stable or the FS is greater than 1.0, whereas the LSF method delineates a zone of potential failure behind the vertical face and near the toe. The potential failure surfaces for

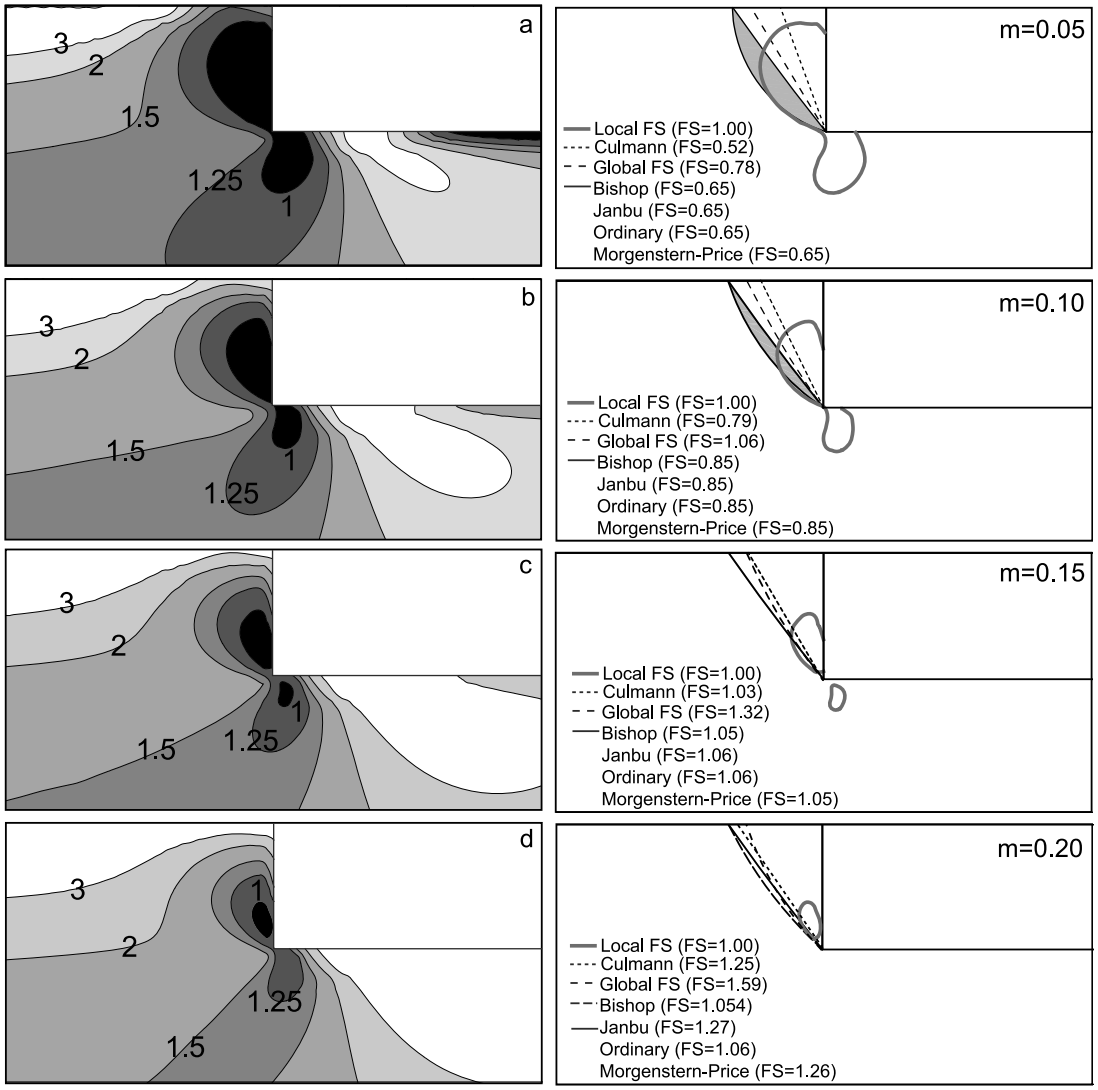

Figure 4. (left) Distribution of the LFS for different stability numbers $m = c'/\gamma H$ calculated using HILLSLOPE $(FS)^2$ for vertical cuts. (right) Comparison of LFS with FS from various limit-equilibrium methods. The black zone in the left column indicates the region where factors of safety are less than 1.0 from the linear elastic analyses. (a) $m = 0.05$, (b) $m = 0.10$, (c) $m = 0.15$, and (d) $m = 0.20$ ($\gamma = 20$ kN/m^3, $\phi' = 30°$).

Janbu, Ordinary, and Morgenstern-Price are identical (thin solid curves), and very close to that given by the global FS in the lower portion of the cut, but different than that by the Bishop method (long dashed curve) in the middle portion of the cut. The potential failure surface predicted by the Culmann method is quite different than the rest of the limit-equilibrium methods. It predicts failure of the cut (short dashed line with FS = 1.0). Note that the lower part of the LFS = 1.0 contour follows closely the potential failure surfaces predicted by the other methods. Overall, Bishop's method yields the lowest FS value (1.054) and is close to the FS given by the Ordinary method (1.06). Both Janbu and Morgenstern's methods yield similar FS values (1.27 versus 1.26), much higher than the FS by Bishop and Ordinary, yet much smaller than the global FS method (1.59).

[23] The fundamental difference between the LFS = 1.0 and the failure surfaces calculated by the different limit-equilibrium methods is that all points along a LFS = 1.0 contour are at the failure state, whereas the state of stress at any point along a FS = 1.0 failure surface from the limit-equilibrium methods may not reach the material strength at that point.

[24] For vertical cuts with a stability number $m = 0.15$ all the limit-equilibrium methods predict the same potential failure surface with nearly identical FS values (1.05 – 1.06). Compared to the case where $m = 0.20$, the Global FS method yields much lower FS value (1.32) and the potential failure surface is farther away from that given by the four limit-equilibrium methods (Figure 4d). Again, the lower part of the LFS = 1.0 contour follows closely the potential failure surfaces predicted by the other methods. Furthermore, the LFS method identifies a failure zone beneath the toe where the LFS is less than unity. As the stability number m decreases (shown respectively for m values of 0.10 and 0.05 in Figures 4b and 4a), all four limit-equilibrium methods predict instability of the vertical cut with the identical FS

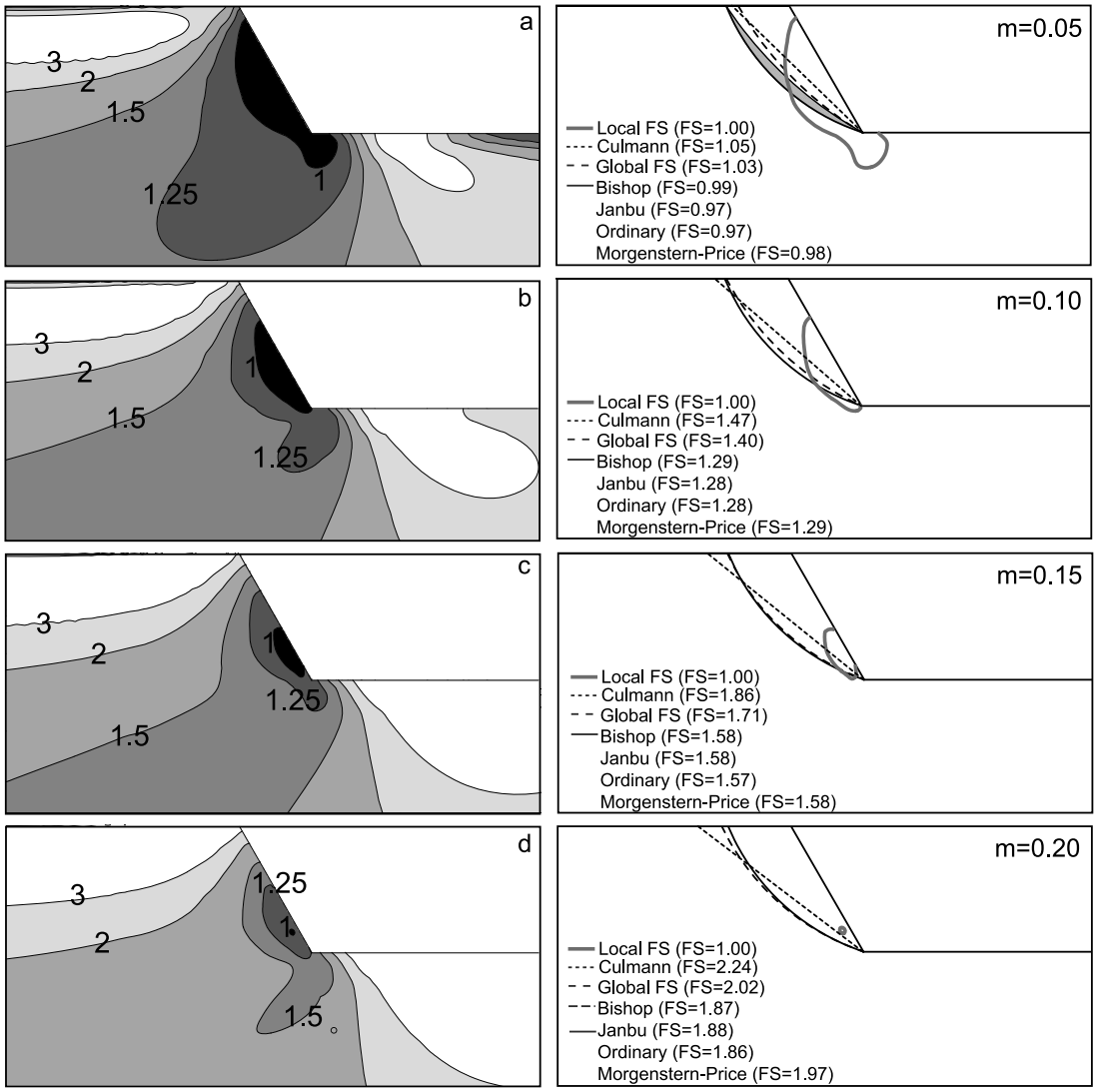

Figure 5. (left) Distribution of the LFS for different stability numbers $m = c'/\gamma H$ calculated using HILLSLOPE (FS)[2] for 60° slopes. (right) Comparison of LFS with FS from various limit-equilibrium methods. The black zone in the left column indicates the region where factors of safety are less than 1.0 from the linear elastic analyses. (a) $m = 0.05$, (b) $m = 0.10$, (c) $m = 0.15$, and (d) $m = 0.20$ ($\gamma = 20$ kN/m^3, $\phi' = 30°$).

value (0.85 for $m = 0.10$ and 0.65 for $m = 0.05$) and similar failure surface. For limit-equilibrium analysis, zones where the FS is less than unity can also be identified and are shown as shaded areas in Figures 4a and 4b. Once again the lower part of the LFS = 1.0 contour follows very closely with the potential failure surfaces predicted by the limit-equilibrium methods. Compared to the potential failure surfaces with higher m values (Figures 4c), both the Global FS and Culmann methods predict nearly identical failure surfaces but away from those by either the limit-equilibrium methods or the LFS method.

[25] In light of the above analysis for the stability of vertical cuts it appears that the failure surface initiates from the toe region behind the vertical face and progresses up-and-left toward the top of the cuts. This trend can only be predicted by the new LFS methodology as the limit-equilibrium methodology explicitly excludes detailed information on the stress distribution and prescribes the failure surface along the general direction of the Rankine's active failure planes, i.e., $\frac{\pi}{4} + \frac{\phi'}{2} = 60°$ where the vertical is the maximum principal stress direction and horizontal the minimum principal stress direction.

4.2. FS and LFS in 60° Slopes

[26] The distributions of LFS are shown in Figure 5 (left) for an example 60° slope. All limit-equilibrium methods produce similar (potential) failure surfaces except for the case of stability number $m = 0.05$ (Figure 5a), where differences near the top of the slope between the limit-equilibrium and the Global FS methods appear. Only one zone with LFS less than unity is identified for all m values. This zone initiates near but above the toe and propagates upward throughout the entire face of the slope as the stability number m decreases. For the stability number $m = 0.20$ (Figure 5d), a zone of LFS less than unity coincides with the potential failure plane predicted by the Culmann method but is located above the potential failure surface predicted by all the limit-equilibrium methods. For the stability number $m =$

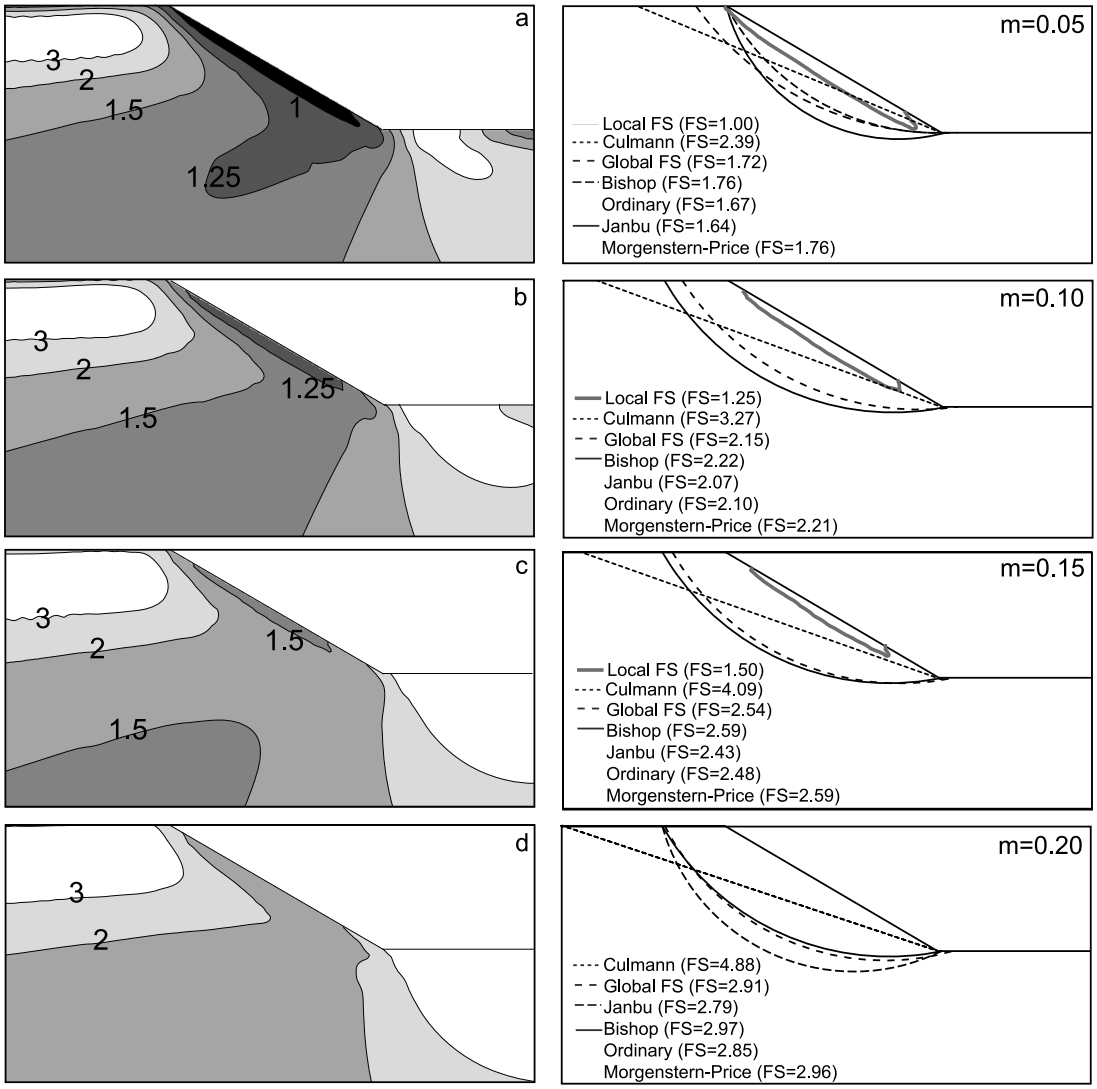

Figure 6. (left) Distribution of the LFS for different stability numbers $m = c'/\gamma H$ calculated using HILLSLOPE (FS)[2] for 30° slopes. (right) Comparison of LFS with FS by various limit-equilibrium methods. The black zone in the left column indicates the region where factors of safety are less than 1.0 from the linear elastic analyses. (a) $m = 0.05$, (b) $m = 0.10$, (c) $m = 0.15$, and (d) $m = 0.20$ ($\gamma = 20$ kN/m^3, $\phi' = 30°$).

0.20 (Figure 5d), $m = 0.15$ (Figure 5c), and $m = 0.10$ (Figure 5b), all the limit-equilibrium methods predict that the slope is stable with similar FS among the four methods. The FS (1.97) is slightly higher for the Morgenstern-Price method for the stability number $m = 0.20$ case and is closer to that given by the Global FS method (FS = 2.02). For the stability number $m = 0.05$ (Figure 5a), the FS predicted by all the limit-equilibrium methods are similar and predict that the slope is unstable (FS < 1.0). However, the global FS method predicts stability (FS = 1.03). The contour of unity for the LFS follows the potential failure surfaces given by the limit-equilibrium methods near the toe for the stability numbers $m = 0.15$ and $m = 0.10$, but is somewhat different for the stability number $m = 0.05$. The contour of unity for the LFS is substantially different compared to the failure surfaces predicted by the limit-equilibrium methods near the crest of the slope. The LFS unity contour exits the domain on the slope face whereas the equilibrium methods predict that the failure surface will intercept the ground surface behind the slope crest. The LFS method predicts failure under conditions where the other methods predict stability providing additional insight into the shape of the failure surface and sensitivity to the distribution of stress. The LFS method predicts small unstable zones on the slope face for the $m = 0.15$ and $m = 0.10$ cases, whereas the limit-equilibrium methods indicate the slope is stable. This implies that the LFS provides an increase in precision and sensitivity in predicting failure geometry over that of the limit-equilibrium methods.

4.3. FS and LFS in 30° Slopes

[27] The trend of larger radii of curvature of the failure surface with decreasing slope gradient predicted by the LFS methodology is examined further in the example showing results for slopes inclined at 30° (Figure 6). The LFS methodology predicts a low FS zone of shallow depth nearly parallel to the slope surface for the slopes with stability numbers of $m = 0.10$ and $m = 0.15$ (Figures 6b and 6c). As the stability number decreases (from Figures 6d to 6a),

this zone progressively elongates and eventually a quasi-translational zone with LFS < 1.0 that encompasses nearly the entire slope surface develops. This pattern of failure is similarly predicted by *Savage*'s [1994] exact solutions for stresses in finite slopes. In contrast, none of the limit-equilibrium methods predict this shape of failure surface or the potential instability for a slope with a stability number $m = 0.05$. The smallest FS calculated by the limit-equilibrium methods is 1.64 (Janbu) and all potential failure surfaces are curved, in contrast to the nearly translational surface predicted by the LFS method. Shallow landslides, typically translational slope failures a few meters thick of unlithified soil mantle or regolith, may dominate mass-movement processes in hillslope environments [*Cruden and Varnes*, 1996; *Trustrum et al.*, 1999; *Sidle and Ochiai*, 2006]. We show that the limit equilibrium-methods do not adequately describe the shape of such failures, whereas the LFS methodology can predict the initiation, evolution, and geometry of such slope failures.

[28] Slope-stability analysis of translational landslides has commonly relied on the infinite-slope model [*e.g.*, *Wu and Sidle*, 1995; *Dietrich et al.*, 1995; *Baum et al.*, 2010], which requires several strict assumptions, including slope-parallel failure surfaces, saturated materials, a sharp contrast between the properties of overlying materials and substrate, and simultaneous failure at given depths. The assumptions of saturated materials, sharp contrast between layered materials, and fixed failure depth have been removed using variably saturated theory for effective stress analysis [*Lu and Godt*, 2008]. Comparison of the LFS methodology with the infinite-slope stability models is presented in the next section for slopes under infiltration conditions.

5. Infiltration-Induced Slope Stability Analysis Using LFS

5.1. Hydrologic Response

[29] Here we use a 30° slope composed of homogeneous silty soil as an example to illustrate the effects of rainfall infiltration on slope stability. The domain and mechanical and hydrologic properties of the hillslope materials are shown in Figure 7a. The surface infiltration boundary is imposed using a 5-month rainfall record for September 2005 to January 2006 collected in the Seattle, Washington, area [*Godt et al.*, 2009] and shown in Figure 7b. This rainfall record is representative of winter season precipitation for coastal regions of the northwestern United States. Soil water retention and suction stress characteristic curves of the silty hillslope are shown in Figure 7c. The water table is set at 5 m below the toe and forms the lower boundary. An initial hydrostatic condition above the water table is imposed, which results in linear variation of soil suction with distance above the water table (not shown) and a nonlinear variation in volumetric soil moisture above the water table (shown in Figure 8a). Both left and right sides of the domain are assumed to be no-flow boundaries. The water table location at the bottom of the domain is fixed.

[30] The variation in soil moisture content resulting from the 5-month rainfall is shown in Figure 8 and Figure 9a. Because the soil near the slope surface is initially quite dry ($\theta < 20\%$) under hydrostatic conditions and the prescribed flux is nearly the same as the saturated hydraulic conductivity, a nearly saturated zone preceded by a sharp wetting front can be observed during the 5-month period (Figures 8b–8d). The progress of the wetting front is also illustrated in Figure 9a as profiles of moisture content at the middle of the slope (A-location in Figure 7a) at different times from the beginning of the rainfall. The wetting front becomes more diffuse as time elapses. Soil suction in the slope changes in a similar pattern to that of the moisture content, as illustrated by the suction profiles at different times in Figure 9b.

[31] The 5-month rainfall episode results in 480 mm water infiltrating into the slope and causes moisture content redistribution throughout the entire slope. The infiltrated water reaches the water table below the toe area in about 112 days, as shown in Figure 8f.

5.2. Mechanical Response

[32] The dynamics of the mechanical response of the slope to the 5-month rainfall period can be quantitatively investigated by examining the suction stress field. Under the framework of the unified effective-stress principle defined in equations (4)–(5), the field of suction stress in the slope can be determined once either the moisture content or soil suction field is known. Figure 10 shows the suction stress field in the slope at different times. Before the rainfall commences, as shown in Figure 9c, suction stress varies nearly linearly with depth below the ground surface and has much smaller absolute values than that of soil suction (shown in Figure 9b) at the same location. For example, near the slope surface at the location **A**, soil suction is −98.0 kPa (Figure 9b) whereas the corresponding suction stress is −34.2 kPa (see Figure 9c). After the rainfall begins, suction stress quickly increases behind the wetting front as shown in Figure 9c and Figures 10b–10f. At the end of December (90 days), a zone with suction stress >−10 kPa is about 0.5 m, as shown in Figure 9c and Figure 10e. After that, suction stress continues to increase in near the slope surface, (Figure 9c and Figures 10f). At the end of the 5-month simulation period (112 days), a zone with suction stress >−10 kPa is about 1.1 m (Figure 9c).

[33] The dynamics of slope stability now can be quantified using the LFS in light of varying field of effective stress in the slope. The field of LFS is calculated simply by using equations (2)–(4) with the field of total stress under the gravity computed from the FEM simulations. The fields of LFS for the slope at different simulation times are shown in Figure 11. Before the rainfall episode, the slope is stable (Figure 11a) and LFS near the slope surface are between 1.50 and 2.00. At 10 days after the rainfall begins, a thin zone nearly parallel to the slope surface with LFS between 1.25 and 1.50 develops (Figure 9d and Figure 11b). At 90 days, a thin zone nearly parallel to the slope surface with LFS less than 1.0 develops. This zone can be identified near the upper middle portion of the slope (Figure 11e). At 112 days, this zone expands to about a maximum thickness of 20 cm near the middle of the slope (Figure 11f and Figure 9d). This zone of LFS < 1.0 spatially and temporally coincides with the large increase in suction stress shown in Figures 10e–10f. Within this zone, as a result of increases in suction stress σ^s or decreases in effective stress (equation (4)), the states of stress shift leftward in in the Mohr diagram (as shown in Figure 2 moving from the solid Mohr circle to the dashed Mohr circle) leading to failure of the soil. It is noteworthy that while the geometry of the moisture content and suction stress contours are more or less parallel to the slope surface (Figures 8

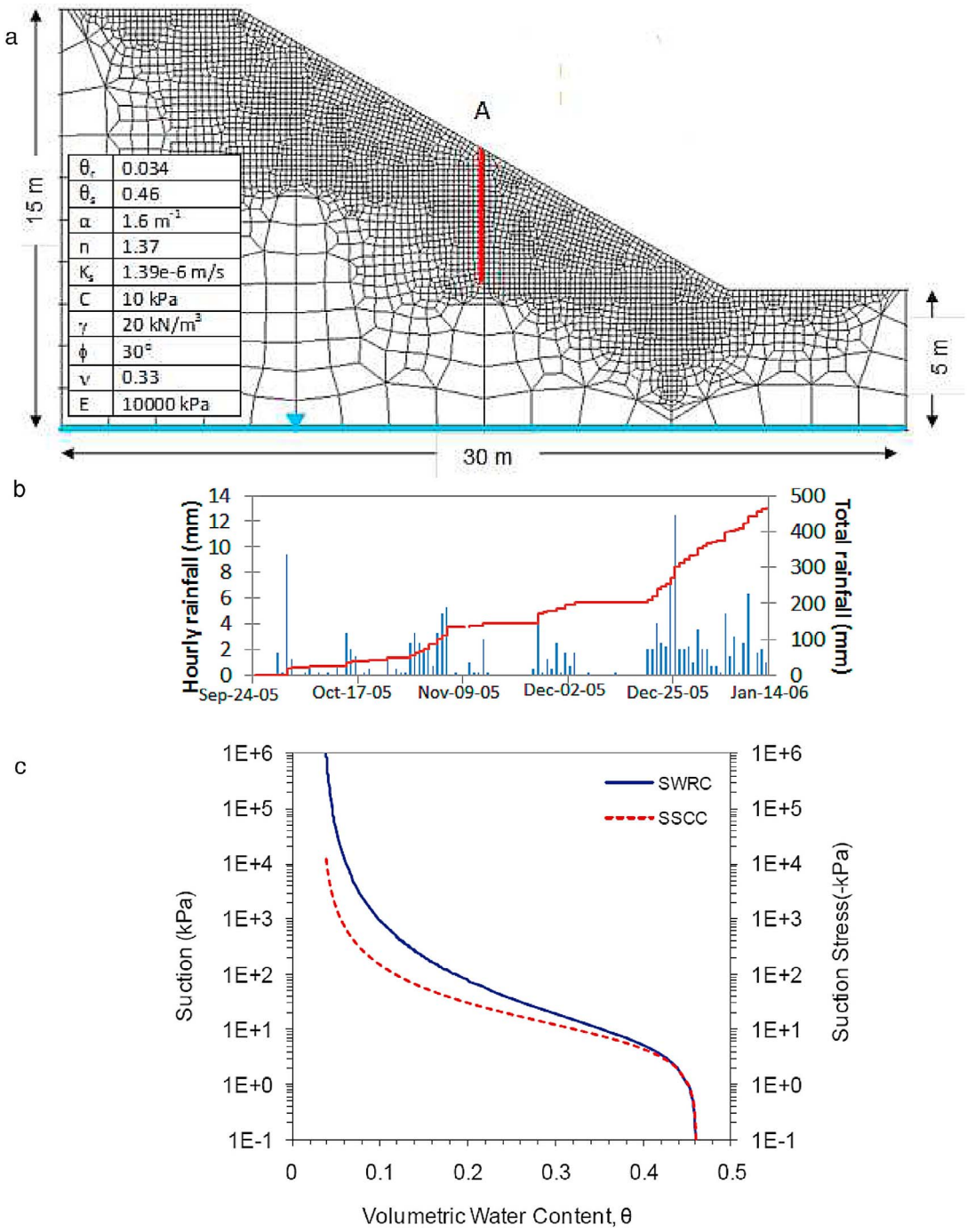

Figure 7. (a) The geometry, material properties and FEM mesh, (b) rainfall scenario from Seattle area recorded during 2005–2006 [*Godt et al.*, 2009], and (c) soil water retention curve (SWRC) and suction stress characteristic curve (SSCC) of the silty soil used in the simulations. Values for residual volumetric water content θ_r, saturated volumetric water content θ_s, *van Genuchten* [1980] parameters, α, n, saturated hydraulic conductivity, K_s, soil cohesion c', moist unit weigh γ, angle of internal friction ϕ', Poisson's ratio ν, and Young's modulus E, are shown in the inset table in Figure 7a.

and 10), the contours of LFS near the slope surface have a lens shape (Figures 11e-11f) that is consistent with field observations of shallow landslides [e.g., *Cruden and Varnes* 1996]. The LFS, as illustrated here, provides quantitative information regarding the initial failure location and a potentially rigorous way to compute the timing, geometry, and progression of potential instability driven by changes in the pore water conditions.

[34] The LFS also provides a quantitative way to examine the suitability of the widely used infinite-slope model for shallow landslides. In recent work by *Lu and Godt* [2008], the infinite-slope stability model was extended to accommodate variably saturated conditions by using the unified

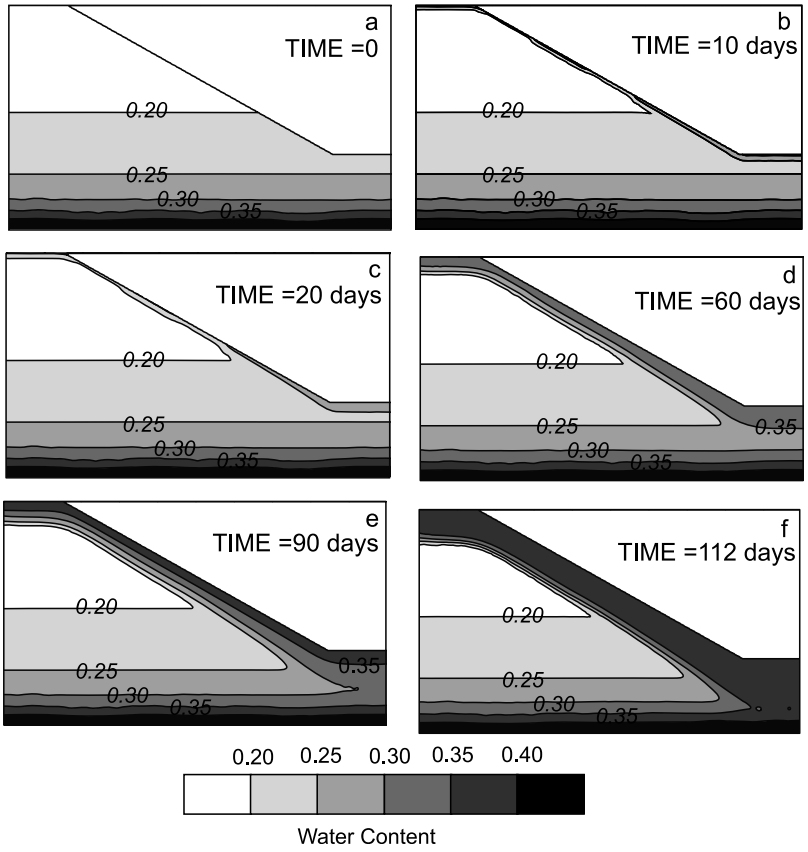

Figure 8. Contours of simulated moisture content at different times for a silty slope under rainfall conditions.

effective stress equation (4) in lieu of Terzaghi's effective stress equation for saturated soil. The FS is [*Lu and Godt*, 2008]

$$F(z,t) = \frac{\tan\phi'}{\tan\beta} + \frac{2c'}{\gamma z \sin 2\beta} - \frac{\sigma^s(z,t)}{\gamma z}(\tan\beta + \cot\beta)\tan\phi' \quad (10)$$

where β is the slope angle, γ is the moist unit weight of soil within the distance z from the slope surface, and t is time. Equation (10) is used to calculate profiles of factor of safety (FS) at location **A** shown in Figure 7a, using the suction stress profiles at different times shown in Figure 9c and the same material strength properties. The calculated FS profiles are shown in Figure 9e and Figure 9f (same with Figure 9e but with different scales in FS values). The FS for the hydrostatic conditions (t = 0) calculated from the infinite-slope stability model increases monotonically from about 2.0 at 3 m below the slope surface to more than 20 near the slope surface (Figure 9e). The monotonic variation pattern is also obtained for cases in which the soil is either dry or saturated in the infinite-slope models. Under unsaturated seepage conditions, the FS profiles are no longer monotonic and the location of minimum FS can occur within unsaturated zone, as illustrated in Figure 9f. *Lu and Godt* [2008] and *Godt et al.* [2009] show that FS could be less than 1.0 in sandy soil on steep slopes under heavy rainfall conditions. For the silty slope after the 5-month rainfall episode, FS can be reduced to less than 3.0 but never reaching 1.0, implying that this slope is stable if infinite-slope theory were used to assess stability. Comparing Figure 9d and Figure 9f, both LFS and the infinite-slope models produce about the same values of FS near 2.0 at relative large distances from the slope surface, where $z > 2.5$ m. However, using the effective stress calculation by FEM (in Figure 9d and Figure 11), the LFS is shown to be less than 1.0 near the slope surface for a certain time period. The overestimation of stability near the slope surface by the infinite slope model compared to the LFS method results from the appearance of distance z in the denominator in equation (10) and is overcome by the new LFS method.

6. Summary and Conclusions

[35] Slope-stability analysis is typically performed by identifying or assuming the potential failure surface and assessing the factor of safety (FS) of that surface. The approach of calculating a single FS for a slope does not provide vital information on how the failure surface initiates and evolves with changes in pore water conditions. A method to calculate a scalar field of FS is proposed based on the concept of Coulomb stress and the shift of stress paths toward the failure state in slopes under variably saturated infiltration and seepage. The FS at each point within a slope is called local factor of safety (LFS) and is defined as the ratio of the adjusted mean stress of the current state of stress to the adjusted mean stress of the potential failure state under the Mohr-Coulomb failure criterion. This LFS includes both compressive and extensional stress failure regimes.

[36] Comparative assessments with the hybrid FEM-limit equilibrium slope stability analyses and stress field-based

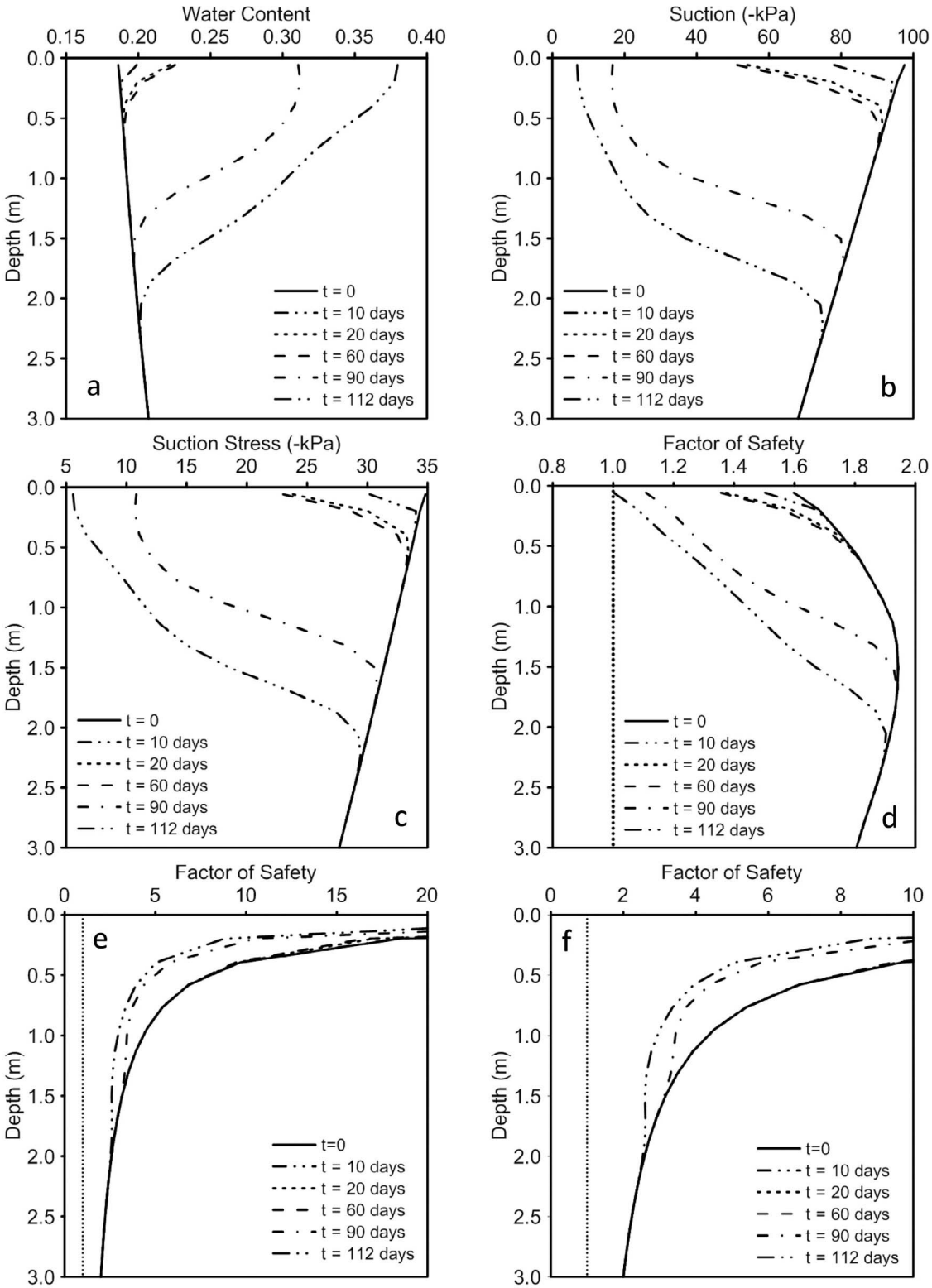

Figure 9. Profiles of (a) moisture content, (b) suction, (c) suction stress, (d) local factor of safety, (e) and (f) factor of safety calculated using an infinite-slope stability analysis in the middle of the silty slope at different times.

FEM-LFS method show that the proposed LFS is consistent with the classic methodologies and yields further insights into the geometry of the potential failure surface and how the failure surface initiates and evolves. From sensitivity analysis of the stability of slopes with various inclined angles and materials, it is shown that the limit-equilibrium methods provide an estimate of stability that exceeds that from the LFS method by a factor up to 2.39 as shown in

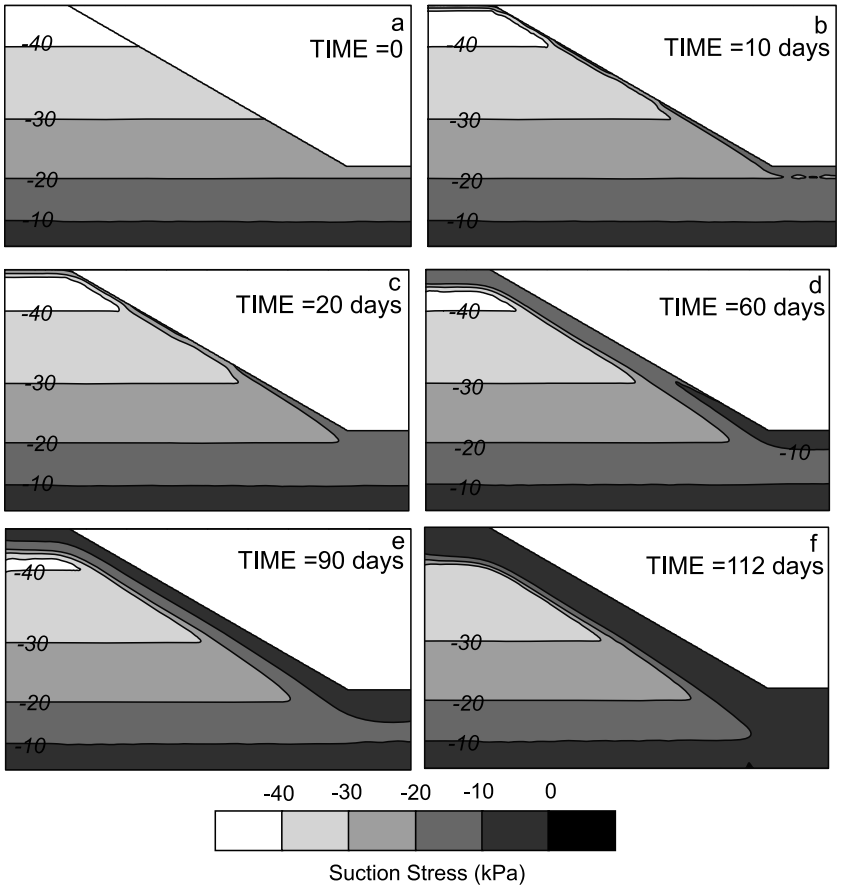

Figure 10. Contours of simulated suction stress at different times for a silty slope under rainfall conditions.

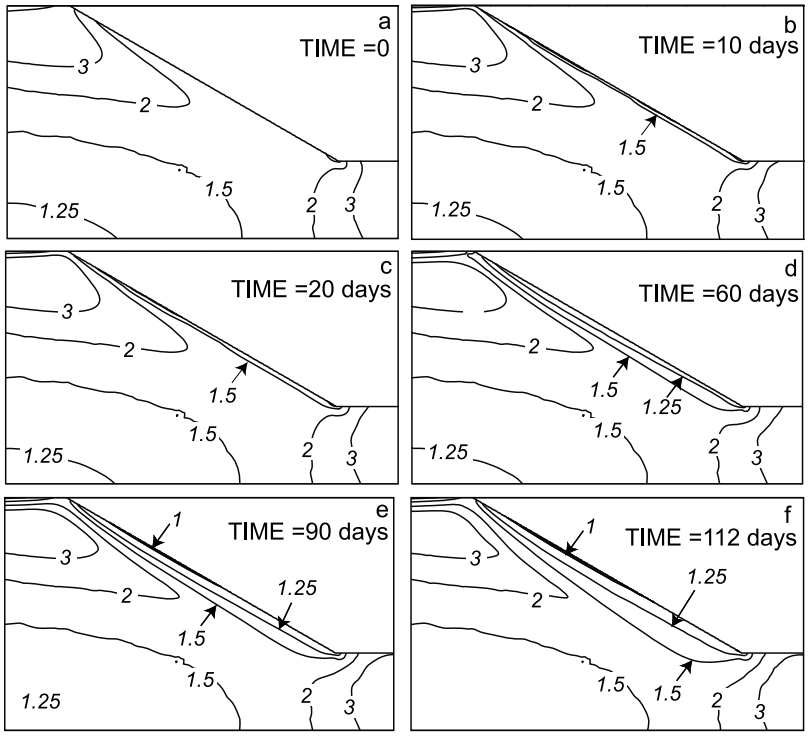

Figure 11. Contours of simulated LFS at different times for a silty slope under rainfall conditions.

Figure 6a. That is, local failure could occur in a slope even if the global FS for the slope is calculated to be 2.39. For steep slopes, while the limit-equilibrium methods produce similar geometries of failure surface near the toe region, they do not capture the geometry of failure surfaces in the middle part of the slope and at higher regions near the crest. For gentle slopes, the limit-equilibrium methods fail to capture both the geometry of the failure surfaces and their occurrence in the near-surface environments.

[37] Quantitative assessments applying the new LFS field method to slopes under infiltration conditions demonstrate that it has a potential to overcome several major limitations in the commonly used global FS methodologies, including accurate prediction of the rupture surface geometry and their occurrence near the slope surface. Comparison with the infinite-slope methods including some recent expansion for variably saturated slope conditions shows further enhancement in predicting shallow landslides by the LFS methodology. Although this work only employs linear elasticity with no postfailure elastoplastic analysis that require more sophisticated elastoplasticity theories, the LFS can provide new perspectives to the stability of slopes for stress field-based methodologies.

[38] **Acknowledgments.** This research is partially supported by a grant from the National Science Foundation (NSF CMMI-0855783) to NL and JWG and a grant from the U.S. Geological Survey (USGS G09AC00085) to NL.

References

Abramson, L. W., T. S. Lee, S. Sharma, and G. M. Boyce (1996), *Slope Stability and Stabilization Methods*, 629 pp., John Wiley, Hoboken, N. J.

Baum, R. L., J. W. Godt, and W. Z. Savage (2010), Estimating the timing and location of shallow rainfall-induced landslides using a model for transient, unsaturated infiltration, *J. Geophys. Res.*, *115*, F03013, doi:10.1029/2009JF001321.

Bishop, A. W. (1955), The use of slip circle in the stability analysis of slopes, *Geotechnique*, *5*(1), 7–17, doi:10.1680/geot.1955.5.1.7.

Cruden, D. M., and D. J. Varnes (1996), Landslide types and processes, in *Landslides: Investigation and Mitigation, Transportation Research Board Special Report*, vol. 247, edited by A. K. Turner and R. L. Schuster, pp. 36–75, Natl. Acad. Press, Washington, D.C.

Culmann, C. (1875), *Die Graphische Statik (Graphic Statics)*, 644 pp., Meyer and Zeller, Zurich.

Dietrich, W. E., R. Reiss, M. L. Hsu, and D. R. Montgomery (1995), A process-based model for colluvial soil depth and shallow landsliding using digital elevation data, *Hydrol. Processes*, *9*(3–4), 383–400, doi:10.1002/hyp.3360090311.

Duncan, J. M. (1996), State of the art: Limit equilibrium and finite-element analysis of slopes, *J. Geotech. Geoenviron. Eng.*, *122*(7), 577–596.

Duncan, J. M., and S. G. Wright (2005), *Soil Strength and Slope Stability*, 309 pp., John Wiley, Hoboken, N. J.

Fellenius, W. (1936), Calculation of the stability of earth dams, in *Transactions of the 2nd Congress on Large Dams*, vol. 4, pp. 445–463, Int. Comm. on Large Dams, Washington, D.C.

Fredlund, D. G., and J. Krahn (1977), Comparison of slope stability methods of analysis, *Can. Geotech. J.*, *14*(3), 429–439, doi:10.1139/t77-045.

Freeze, R. A., and J. A. Cherry (1979), *Groundwater*, 604 pp., Prentice Hall, Englewood Cliffs, New Jersey.

GEO-SLOPE International (2007), *GeoStudio*, Calgary, Alberta, Canada.

Godt, J. W., R. L. Baum, and N. Lu (2009), Landsliding in partially saturated materials, *Geophys. Res. Lett.*, *36*, L02403, doi:10.1029/2008GL035996.

Iverson, R. M., and M. E. Reid (1992), Gravity-driven groundwater flow and slope failure potential 1. Elastic effective-stress model, *Water Resour. Res.*, *28*(3), 925–938, doi:10.1029/91WR02694.

Janbu, N. (1973), Slope stability computations. Embankment-dam engineering, in *Casagrande*, vol. R, edited by C. Hirschfeld and S. J. Poulos, pp. 49–86, John Wiley, New York.

King, G. C. P., R. S. Stein, and J. Lin (1994), Static stress changes and the triggering of earthquakes, *Seismol. Soc. Am. Bull.*, *84*, 935–953.

Krahn, J. (2003), The 2001 R.M. Hardy Lecture: the limits of limit equilibrium analyses, *Can. Geotech. J.*, *40*, 643–660, doi:10.1139/t03-024.

Lade, P. V. (1992), Static instability and liquefaction of loose fine sandy slopes, *J. Geotech. Eng.*, *118*(1), 51–71, doi:10.1061/(ASCE)0733-9410(1992)118:1(51).

Lohnes, R. A., and R. L. Handy (1968), Slope angle in friable loess, *J. Geol.*, *76*(3), 247–258, doi:10.1086/627327.

Lu, N., and J. W. Godt (2008), Infinite slope stability under unsaturated seepage conditions, *Water Resour. Res.*, *44*, W11404, doi:10.1029/2008WR006976.

Lu, N., and D. V. Griffiths (2004), Profiles of steady-state suction stress in unsaturated soils, *J. Geotech. Geoenviron. Eng.*, *130*(10), 1063–1076, doi:10.1061/(ASCE)1090-0241(2004)130:10(1063).

Lu, N., and W. J. Likos (2004), *Unsaturated Soil Mechanics*, 584 pp., John Wiley, New York.

Lu, N., and W. J. Likos (2006), Suction stress characteristic curve for unsaturated soils, *J. Geotech. Geoenviron. Eng.*, *132*(2), 131–142, doi:10.1061/(ASCE)1090-0241(2006)132:2(131).

Lu, N., A. Wayllace, and J. W. Godt (2010a), A hydro-mechanical model for predicting infiltration-induced landslides, paper presented at 2010 Modeling Conference, U. S. Geol. Soc., Bloomfield, Colo.

Lu, N., J. Godt, and D. T. Wu (2010b), A closed-form equation for effective stress in unsaturated soil, *Water Resour. Res.*, *46*, W05515, doi:10.1029/2009WR008646.

Malvern, L. E. (1969), *Introduction to the Mechanics of a Continuous Medium*, Prentice-Hall, Upper Saddle River, N. J.

Matsui, T., and K. C. San (1992), Finite element slope stability analysis by shear strength reduction technique, *Soil Found.*, *32*(1), 59–70, doi:10.3208/sandf1972.32.59.

Michalowski, R. L. (2002), Stability charts for uniform slopes, *J. Geotech. Geoenviron. Eng.*, *128*(4), 351–355, doi:10.1061/(ASCE)1090-0241(2002)128:4(351).

Morgenstern, N. R., and V. E. Price (1965), The analysis of the stability of general slip surface, *Geotechnique*, *15*(4), 289–290.

Mualem, Y. (1976), Hysteretical models for prediction of the hydraulic conductivity of unsaturated porous media, *Water Resour. Res.*, *12*(6), 1248–1254, doi:10.1029/WR012i006p01248.

Reddy, J. N. (1985), *Introduction to the Finite Element Method*, McGraw-Hill, New York.

Savage, W. Z. (1994), Gravity-induced stress in finite slopes, *Int. J. Mech. Min. Sci. Geomech. Abstr.*, *31*(5), 471–483, doi:10.1016/0148-9062(94)90150-3.

Sidle, R. C., and H. Ochiai (Eds.) (2006), Landslides: Processes, Prediction, and Land Use, in *Water Resour. Monogr.*, vol. 18, 312 pp., AGU, Washington D.C.

Simunek, J., T. Vogel, and M. T. van Genuchten (1994), The SWMS-2D code for simulating water flow and solute transport in two-dimensional variably saturated media, Version 1.21, *Res. Rep. 132*, USDA-ARS U.S. Salinity Lab., Riverside, Calif.

Smith, I. M., and D. V. Griffiths (2004), *Programming the Finite Element*, 4th ed., John Wiley, West Sussex, U. K.

Swan, C. C., and Y. K. Seo (1999), Limit state analysis of earthen slopes using dual continuum/FEM approaches, *Int. J. Numer. Anal. Methods Geomech.*, *23*(12), 1359–1371, doi:10.1002/(SICI)1096-9853(199910)23:12<1359::AID-NAG39>3.0.CO;2-Y.

Toda, S., R. S. Stein, P. A. Reasenberg, J. H. Dieterich, and A. Yoshida (1998), Stress transferred by the 1995 M_ω = 6.9 Kobe, Japan, shock: Effect on aftershocks and future earthquake probabilities, *J. Geophys. Res.*, *103*(B10), 24,543–24,565, doi:10.1029/98JB00765.

Trustrum, N. A., B. Gomez, M. J. Page, L. M. Reid, and D. M. Hicks (1999), Sediment production, storage and output: The relative role of large magnitude events in steepland catchments, *Z. Geomorphol. Suppl.*, *115*, 71–86.

van Genuchten, M. T. (1980), A closed form equation for predicting the hydraulic conductivity of unsaturated soils, *Soil Sci. Soc. Am. J.*, *44*, 892–898, doi:10.2136/sssaj1980.03615995004400050002x.

Wu, W., and R. C. Sidle (1995), A distributed slope stability model for steep forested basins, *Water Resour. Res.*, *31*(8), 2097–2110, doi:10.1029/95WR01136.

Yu, H. S., R. Salgado, S. Sloan, and J. Kim (1998), Limit analysis versus limit equilibrium for slope stability assessment, *J. Geotech. Geoenviron. Eng.*, *124*(1), 1–11, doi:10.1061/(ASCE)1090-0241(1998)124:1(1).